Collapse and Fragmentation of Molecular Cloud Cores. X. Magnetic Braking of Prolate and Oblate Cores.

Alan P. Boss

Department of Terrestrial Magnetism, Carnegie Institution of Washington, 5241 Broad Branch Road, NW, Washington, DC 20015-1305

`boss@dtm.ciw.edu`

ABSTRACT

The collapse and fragmentation of initially prolate and oblate, magnetic molecular clouds is calculated in three dimensions with a gravitational, radiative hydrodynamics code. The code includes magnetic field effects in an approximate manner: magnetic pressure, tension, braking, and ambipolar diffusion are all modelled. The parameters varied for both the initially prolate and oblate clouds are the initial degree of central concentration of the radial density profile, the initial angular velocity, and the efficiency of magnetic braking (represented by a factor $f_{mb} = 10^{-4}$ or 10^{-3}). The oblate cores all collapse to form rings that might be susceptible to fragmentation into multiple systems. The outcome of the collapse of the prolate cores depends strongly on the initial density profile. Prolate cores with central densities 20 times higher than their boundary densities collapse and fragment into binary or quadruple systems, whereas cores with central densities 100 times higher collapse to form single protostars embedded in bars. The inclusion of magnetic braking is able to stifle protostellar fragmentation in the latter set of models, as when identical models were calculated without magnetic braking (Boss 2002), those cores fragmented into binary protostars. These models demonstrate the importance of including magnetic fields in studies of protostellar collapse and fragmentation, and suggest that even when magnetic fields are included, fragmentation into binary and multiple systems remains as a possible outcome of protostellar collapse.

Subject headings: hydrodynamics — ISM: clouds — ISM: kinematics and dynamics — MHD — stars: formation

1. Introduction

Fragmentation during protostellar collapse is widely accepted to be the primary mechanism for the formation of binary and multiple star systems (e.g., Lafrenière et al. 2008; Chen et al. 2008). While it is clear that the overall form of the initial mass function for stars is directly tied to the initial conditions for protostellar collapse, i.e., the mass function of dense cloud cores (e.g., Dib et al. 2008; Swift & Williams 2008), fragmentation is necessary for producing binary star systems within these individual dense cores (Lafrenière et al. 2008; Chen et al. 2008).

Three dimensional calculations of the collapse of centrally condensed, rotating cloud cores have been computed for quite some time (e.g., Boss 1993) and continue to attract theoretical attention (e.g., Saigo et al. 2008; Machida 2008; Commercon et al. 2008). These calculations neglected the effects of magnetic fields. However, observations of OH Zeeman splitting in dark cloud cores have shown that magnetic fields are often an important contributer to cloud support against collapse for densities in the range of $10^3 - 10^4$ cm^{-3} (Troland & Crutcher 2008). Given this observational constraint, it is clear that three dimensional hydrodynamical collapse calculations should include magnetic field effects as well as self-gravity and radiative transfer (e.g., Boss 1997, 1999, 2002, 2005, 2007). Magnetic fields are now being included in other three dimensional collapse models as well (e.g., Machida et al. 2004, 2005a,b, 2007, 2008; Kudoh et al. 2007; Price & Bate 2007, 2008). In particular, Price & Bate (2007) found that while magnetic pressure acts to resist fragmentation during collapse, magnetic tension can actually aid fragmentation, confirming the results found by Boss (2002). Machida et al. (2004, 2005a,b, 2007, 2008) generally found that binary fragmentation could still occur provided that the initial magnetic cloud core rotated fast enough.

Magnetic braking is effective at reducing cloud rotation rates during the pre-collapse cloud phase, but has relatively little effect during the collapse phase, according to the two dimensional magnetohydrodynamics models of Basu & Mouschovias (1994, 1995a,b). However, Hosking & Whitworth (2004) found that rotationally-driven fragmentation could be halted by magnetic braking during the collapse phase. Boss (2004) argued that the thermodynamical treatment employed by Hosking & Whitworth (2004) could have been more important for stifling fragmentation than magnetic braking, but did not offer any models of magnetic braking to support this assertion.

Price & Bate (2007) presented models of the collapse of magnetic cloud cores, finding that magnetic pressure was more important for inhibiting fragmentation than either magnetic tension or braking, contrary to the results presented by Hosking & Whitworth (2004) and Fromang et al. (2006), who found no evidence at all for the fragmentation of magnetic clouds.

Fromang et al. (2006) assumed ideal magnetohydrodynamics (MHD), i.e., without ambipolar diffusion, a fact that is likely to stifle fragmentation, whereas Hosking & Whitworh (2004), Boss (2004), and Price & Bate (2007) included ambipolar diffusion. However, subsequent ideal MHD collapse calculations by Hennebelle & Fromang (2008) and Hennebelle & Teyssier (2008) found that magnetic clouds could fragment if the initial density perturbation was large enough, and they speculated on what would happen if ambipolar diffusion was included in their models. These fundamental differences in the results of magnetic cloud collapse calculations results highlight the need to compare models where only one parameter at a time is being changed, so that the true effect of changing that one parameter can be discerned. Such a comparison is the major goal of the present study.

Banerjee & Pudritz (2006) considered the collapse of magnetized cloud cores, finding that even though considerable angular momentum was lost from the cloud core by magnetic outflows from the disk's surface, the cloud was still able to collapse and fragment into a close binary protostar system.

Price & Bate (2007) and Hennebelle & Teyssier (2008) both considered the collapse of spherical, magnetic cloud cores with initially uniform density and uniform magnetic field strengths. Machida et al. (2004, 2005a,b) studied the collapse of initially cylindrical cloud cores in hydrostatic equilibrium. Machida et al. (2008) considered the collapse of cloud cores with density profiles appropriate for Bonnor-Ebert isothermal spheres, similar to the Gaussian radial density profile clouds studied by Boss (1997, 2002) and by this paper. Such centrally-condensed density profiles represent the best guesses as to the radial structure of pre-collapse molecular cloud cores (e.g., Myers et al. 1991; Ward-Thompson, Motte, & André 1999).

Boss (2002) modelled the collapse of initially prolate and oblate cores, including several magnetic field effects, but ignoring magnetic braking. Prolate and oblate cloud shapes have been inferred from observations of suspected pre-collapse molecular cloud cores (e.g., Jones, Basu, & Dubinski 2001; Curry & Stahler 2001). Here we use the magnetic braking approximation developed by Boss (2007), originally applied to filamentary clouds, to examine the importance of magnetic braking for the same prolate and oblate models as those calculated by Boss (2002), allowing a direct comparison between identical protostellar collapse models with and without magnetic braking. These models thus directly address the different outcomes of the models with magnetic braking but without detailed thermodynamics by Hosking & Whitworth (2004) compared to those without magnetic braking but with detailed thermodynamics of Boss (2004): the present models include both effects.

2. Numerical Methods

The numerical models are calculated with a three-dimensional hydrodynamics code that calculates finite-difference solutions of the equations of radiative transfer, hydrodynamics, and gravitation for a compressible fluid (Boss & Myhill 1992). The hydrodynamic equations are solved in conservation law form on a contracting spherical coordinate grid, subject to constant volume boundary conditions on the spherical boundary. The code is second-order-accurate in both space and time, with the van Leer-type hydrodynamical fluxes having been modified to improve stability (Boss 1997). Artificial viscosity is not employed. Radiative transfer is handled in the Eddington approximation, including detailed equations of state and dust grain opacities (e.g., Pollack et al. 1994). The code has been tested on a variety of test problems (Boss & Myhill 1992; Myhill & Boss 1993).

The Poisson equation for the cloud's gravitational potential is solved by a spherical harmonic expansion (Y_{lm}) including terms up to $N_{lm} = 32$. The computational grid consists of a spherical coordinate grid with $N_r = 200$, $N_\theta = 22$ for $\pi/2 \geq \theta > 0$ (symmetry through the midplane is assumed for $\pi \geq \theta > \pi/2$), and $N_\phi = 256$ for $2\pi \geq \phi \geq 0$, i.e., with no symmetry assumed in ϕ. The radial grid contracts to follow the collapsing inner regions and to provide sufficient spatial resolution to ensure satisfaction of the four Jeans conditions for a spherical coordinate grid (Truelove et al. 1997; Boss et al. 2000). The innermost 50 radial grid points are kept uniformly spaced during grid contraction, while the outermost 150 are non-uniformly spaced, in order to provide an inner region with uniform spatial resolution in the radial coordinate. The ϕ grid is uniformly spaced, whereas the θ grid is compressed toward the midplane, where the minimum grid spacing is 0.3 degrees.

3. Initial Conditions

Tables 1 and 2 list the initial conditions for the models. The initial models have Gaussian radial density profiles (Boss 1997) of the form

$$\rho_i(x, y, z) = \rho_o \, exp\left(-\left(\frac{x}{r_a}\right)^2 - \left(\frac{y}{r_b}\right)^2 - \left(\frac{z}{r_c}\right)^2\right), \tag{1}$$

where $\rho_0 = 2.0 \times 10^{-18}$ g cm^{-3} is the initial central density. The prolate clouds with central densities 20 times higher than a reference boundary density have $r_a = 1.16R$ and $r_b = r_c = 0.580R$, where R is the cloud radius, yielding a axis ratio of 2 to 1. The oblate clouds with the same degree of central concentration have $r_a = r_b = 1.16R$ and $r_c = 0.580R$. For 100 to 1 density contrasts, the prolate clouds have $r_a = 0.932R$ and $r_b = r_c = 0.466R$, while the

oblate clouds have $r_a = r_b = 0.932R$ and $r_c = 0.466R$. Random numbers $(ran(x, y, z))$ in the range [0,1] are used to add noise to these initial density distributions by multiplying ρ_i from the above equation by the factor $[1 + 0.1 \ ran(x, y, z)]$. The cloud radius is $R = 1.0 \times 10^{17}$ cm ≈ 0.032 pc for all models.

The cloud masses are 1.5 $M_\odot$ and 2.1 $M_\odot$, respectively, for the prolate and oblate clouds with a 20:1 density ratio, and 0.96 $M_\odot$ and 1.5 $M_\odot$, for the prolate and oblate clouds with a 100:1 density ratio. With an initial temperature of 10 K, the initial ratio of thermal to gravitational energy is $\alpha_i = 0.39$ for the prolate clouds and 0.30 for the oblate clouds with the 20:1 initial density ratio, while $\alpha_i = 0.55$ for the prolate clouds and 0.39 for the oblate clouds with the 100:1 initial density ratio.

Solid body rotation is assumed, with the angular velocity about the $\hat{z}$ axis (short axis) taken to be $\Omega_i = 10^{-14}, 3.2 \times 10^{-14}$, or 10^{-13} rad s^{-1}. These choices of Ω_i result in initial ratios of rotational to gravitational energy varying from $\beta_i = 1.2 \times 10^{-4}$ to 0.015 for the prolate clouds and $\beta_i = 1.1 \times 10^{-4}$ to 0.013 for the oblate clouds. These choices are all consistent with observational constraints on the densities, shapes, and rotation rates of dense cloud cores (e.g., Myers et al. 1991; Goodman et al. 1993; Ward-Thompson, Motte, & André 1999; Jones, Basu, & Dubinski 2001; Curry and Stahler 2001).

As in the previous three-dimensional models (Boss 1997, 1999, 2002, 2005, 2007), the effects of magnetic fields are approximated through the use of several simplifying approximations regarding magnetic pressure, tension, braking, and ambipolar diffusion (see Boss 2007 for a derivation of these approximations). All models assumed an ambipolar diffusion time scale $t_{ad} = 10 \ t_{ff}$, where the free fall time $t_{ff} = (3\pi/32G\rho_0)^{1/2} = 4.7 \times 10^4$ yr for a central density $\rho_0 = 2.0 \times 10^{-18}$ g cm^{-3}. The reference magnetic field strength is assumed to be $B_{oi} = 200\mu$G. The magnetic braking factor f_{mb} is taken to be either 0.0001 or 0.001. Based on the models of Basu & Mouschovias (1994), Boss (2007) estimated that $f_{mb} \sim 0.0001$. The models with $f_{mb} = 0.001$ are thus intended to attempt to overestimate the effects of magnetic braking.

Note, however, that the calculations of Basu & Mouschovias (1994) stopped at central densities of 3×10^9 cm^{-3}, i.e., before the clouds became optically thick, whereas the present models are continued well in the optically thick regime. Hence the implicit assumption that the trends found in the Basu & Mouschovias (1994) models and used by Boss (2007) to derive the f_{mb} approximation should continue indefinitely may not be warranted, though the trends do persist over the previous six orders of magnitude increase in central density of their models (see Figure 7 of Basu & Mouschovias 1994). The magnetic braking studied by Basu & Mouschovias (1994) is similar to the magnetic braking produced by disk jets and outflows in the models by Banerjee & Pudritz (2006), Hennebelle & Fromang (2008), and

Hennebelle & Teyssier (2008). A superior treatment of magnetic braking beyond the f_{mb} approximation of Boss (2007) will require a true MHD code.

With the field strength $B_{oi} = 200\mu$G, the prolate or oblate clouds with 20:1 density contrasts have initial ratios of magnetic to gravitational energy of $\gamma_i = 0.58$ or 0.43, respectively. For density ratios of 100:1, $\gamma_i = 0.81$ for the prolate clouds and 0.57 for the oblate clouds. The mass to flux ratio of these clouds is less than the critical mass to flux ratio, making all the clouds formally magnetostatically stable and hence magnetically subcritical. Protostellar collapse cannot occur until ambipolar diffusion leads to sufficient loss of magnetic field support for sustained contraction to begin.

4. Results

Tables 1 and 2 list the initial conditions as well as the basic outcome of each model, namely the final time to which the cloud was advanced t_f (in units of the initial cloud free fall time) and whether the cloud collapsed to form a quadruple system (Q), binary (B), binary-bar (BB), single-bar (SB), ring (R), or did not collapse (NC). For convenience, the results of the corresponding models by Boss (2002) without magnetic braking are shown as well.

Figure 1 shows the initial equatorial density distribution for the prolate cores with a 20:1 density contrast. Given the stability of the initial models, evolutions consist of the clouds oscillating about the initial configurations, waiting for sufficient time to elapse for ambipolar diffusion to reduce the magnetic field support enough to allow collapse to proceed, as in the previous magnetic cloud models (e.g., Boss 1997). Figure 2 shows the result for model P2BB, which collapsed to form a quadruple protostellar system, though in this case with an additional central density maximum. Without magnetic braking, this core collapsed to form a binary protostar system, so in this case magnetic braking has led to an increased degree of fragmentation. The off-axis clump evident in Figure 2 at 9 o'clock has a maximum density of 2.5×10^{-12} g cm^{-3} and an average temperature of 20 K. Considering regions with a density at least 0.1 that of this maximum density, the clump's mass is 2.6 Jupiter masses, greater than the Jeans mass at that density and temperature of 1.9 Jupiter masses. The ratio of thermal to gravitational energy for the clump is 0.49, showing that it is gravitationally bound. The ratio of rotational to gravitational energy is 0.39, so the clump is in rapid rotation. These fragment properties are quite similar to those found in the Boss (2002) models.

Model P2BA behaved in much the same way as P2BB, even with stronger magnetic braking ($f_{mb} = 0.001$ for P2BA compared to $f_{mb} = 0.0001$ for P2BB).

Figure 3 shows the outcome of model P2BD, which started with a lower initial angular velocity than model P2BB but was otherwise identical. In this case, a well-defined binary protostar system forms. A similar outcome resulted for model P2BC with a higher degree of magnetic braking. With even lower initial angular velocity than P2BC and P2BD, model P2BE collapsed to form a binary-bar system (Figure 4), i.e., a binary with its members connected by a bar of rotating gas. In the case of model P2BE, there are two density maxima in the bar near the center of the system, possible evidence for further fragments, though none of the density maxima are as well-defined as those of the binary in Figure 3. In contrast, when magnetic braking was neglected (Boss 2002), a core identical to model P2BE fragmented into a well-defined binary system, so in this case magnetic braking has reduced the degree of fragmentation.

The prolate core models with 100:1 initial density contrasts all behaved in the same manner and formed single central protostars embedded in bar-like structures. Figure 5 shows the result for model P1BB, termed a single-bar. Figure 6 shows the equatorial temperature contours for this model, emphasizing the highly non-uniform temperature distribution that results from including radiative transfer effects (e.g., Boss et al. 2000). The temperature field is strongest in regions where the infalling gas is forming shock-like density corrugations, yielding an x-shaped pattern in the cloud's midplane. The formation of single-bars in all five of the prolate 100:1 models compared to the formation of binaries in the corresponding Boss (2002) models shows that when the initial cores are highly centrally condensed, magnetic braking is able to frustrate fragmentation.

Figure 7 shows the initial conditions for the oblate cores with 20:1 initial density contrasts, while Figure 8 depicts the outcome of model O2BB: a well-defined ring. While the ring shows no particular tendency to fragment over the time scale of the calculation, such a configuration is expected to fragment eventually. With the exception of model O2BA, which did not collapse significantly, all of the oblate cores collapsed to form rings, for both 20:1 and 100:1 density contrasts, though the rings were more pronounced for the cores with higher initial rotation rates, such as O2BB in Figure 8. In comparison, the corresponding Boss (2002) models formed a combination of rings or rings which showed a tendency to fragment into quadruple systems. Hence the oblate cloud models indicate that the inclusion of magnetic braking had only a mild tendency to inhibit their fragmentation.

Tables 1 and 2 show that the prolate clouds tended to take considerably longer to undergo collapse than the oblate clouds, implying a considerably longer period in the pre-collapse, quasi-equilibrium phase where thermal and magnetic support dominate. As a result, the effect of magnetic braking through the f_{mb} approximation should be stronger in the models which took the longest time to collapse, i.e., the models in Table 1 with $\rho_0/\rho_R =$

$100 : 1$ and $t_f/t_{ff} \sim 9$. Prolonged magnetic braking will tend to suppress rotationally-driven fragmentation, consistent with the formation of single-bars for the prolate models in Table 1 with $t_f/t_{ff} \sim 9$. Model P2bb, for example, lost about 0.4% of its total angular momentum during its evolution to $t_f/t_{ff} = 4.683$, compared to a loss of about 1% for model P1Bb within $t_f/t_{ff} = 9.071$. Note though that for the oblate models in Table 2, no such effect is evident, perhaps because all of those models collapsed within $t_f/t_{ff} < 5$. In fact, a comparision of the corresponding oblate models shows that model O2bb lost about 0.4% of its total angular momentum during its evolution to $t_f/t_{ff} = 2.456$, compared to a loss of about 1% for model O1Bb within $t_f/t_{ff} = 4.636$. Both models O2BB and O1BB collapse to form rings. Their percentage angular momentum losses are identical to those for models P2BB and P1BB, which formed a quadruple and single-bar, respectively, implying that the initial cloud shape and degree of central concentration do have an important effect on the fragmentation process of magnetic clouds.

5.   Conclusions

These pseudo-magnetohydrodynamics calculations have explored the possibly deleterious effects of magnetic braking on protostellar fragmentation, an issue explored by Hosking & Whitworth (2004). A degree of inhibition of fragmentation caused by magnetic braking of both prolate and oblate, dense cloud cores has been identified in these models through a direct comparison with otherwise identical models calculated by Boss (2002) without magnetic braking. Nevertheless, a cursory examination of the figures and tables reveals that there is a still a large portion of initial conditions space that appears to be permissive of fragmentation of magnetic clouds when the approximate effects of magnetic pressure, tension, and braking are all included. The present models thus suggest that binary and multiple stars may well form from the collapse and fragmentation of magnetic, as well as non-magnetic, dense cloud cores, though perhaps not quite so readily.

Given the approximate nature of the present calculations (Boss 2007), it will be important to try to confirm these results with a true magnetohydrodynamics code. This could be accomplished by adding a numerical solution of the magnetic induction equation to the Boss & Myhill (1992) code. Alternatively, these calculations could be repeated using publically available MHD codes, such as the FLASH adaptive mesh refinement code (e.g., Duffin & Pudritz 2008), though FLASH does not at present include Eddington approximation radiative transfer, unlike the Boss & Myhill (1992) code. Attempting such true MHD calculations stands as a challenge for future work on the question of protostellar collapse and fragmentation.

REFERENCES

Banerjee, R., & Pudritz, R. E. 2006, ApJ, 641, 949

Basu, S., & Mouschovias, T. Ch. 1994, ApJ, 432, 720

——. 1995a, ApJ, 452, 386

——. 1995b, ApJ, 453, 271

Boss, A. P. 1993, ApJ, 410, 157

——. 1997, ApJ, 483, 309

——. 1999, ApJ, 520, 744

——. 2002, ApJ, 568, 743

——. 2004, MNRAS, 350, L57

——. 2005, ApJ, 622, 393

——. 2007, ApJ, 658, 1136

Boss, A. P., Fisher, R. T., Klein, R. I., & McKee, C. F. 2000, ApJ, 528, 325

Boss, A. P., & Myhill, E. A. 1992, ApJS, 83, 311

Chen, X., Launhardt, R., Bourke, T., Henning, T., & Barnes, P. J. 2008, ApJ, 683, 862

Commercon, B., Hennebelle, P., Audit, E., Chabrier, G., & Teyssier, R. 2008, A&A, 482, 371

Curry, C. L., & Stahler, S. W. 2001, ApJ, 555, 160

Dib, S., Brandenburg, A., Kim, J., Gopinathan, M., & André, P. 2008, ApJ, 678, L105

Duffin, D. F., & Pudritz, R. E. 2008, MNRAS, in press

Fromang, S., Hennebelle, P., & Teyssier, R. 2006, A&A, 457, 371

Goodman, A. A., Benson, P. J., Fuller, G. A., & Myers, P. C. 1993, ApJ, 406, 528

Hennebelle, P., & Fromang, S. 2008, A&A, 477, 9

Hennebelle, P., & Teyssier, R. 2008, A&A, 477, 25

Hosking, J. G., & Whitworth, A. P. 2004, MNRAS, 347, 1001

Jones, C. E., Basu, S., & Dubinski, J. 2001, ApJ, 551, 387

Kudoh, T., Basu, S., Ogata, Y., & Yabe, T. 2007, MNRAS, 380, 499

Lafrenière, D., Jayawardhana, R., Brandeker, A., Ahmic, M., & van Kerkwijk, M. H. 2008, ApJ, 683, 844

Machida, M. N. 2008, ApJ, 682, L1

Machida, M. N., Tomisaka, K., & Matsumoto, T. 2004, MNRAS, 348, L1

Machida, M. N., Matsumoto, T., Tomisaka, K., & Hanawa, T. 2005a, MNRAS, 362, 369

Machida, M. N., Matsumoto, T., Hanawa, T., & Tomisaka, K. 2005b, MNRAS, 362, 382

Machida, M. N., Inutsuka, S.-I, & Matsumoto, T. 2007, ApJ, 670, 1198

Machida, M. N., Tomisaka, K., Matsumoto, T., & Inutsuka, S.-I 2008, ApJ, 677, 327

Myers, P. C., Fuller, G. A., Goodman, A. A., & Benson, P. J. 1991, ApJ, 376, 561

Myhill, E. A., & Boss, A. P. 1993, ApJS, 89, 345

Pollack, J. B., Hollenbach, D., Beckwith, S., Simonelli, D. P., Roush, T., & Fong, W. 1994, ApJ, 421, 615

Price, D. J., & Bate M. R. 2007, MNRAS, 377, 77

——. 2008, MNRAS, 385, 1820

Saigo, K., Tomisaka, K., & Matsumoto, T. 2008, ApJ, 674, 997

Swift, J. J., & Williams, J. P. 2008, ApJ, 679, 552

Troland, T. H., & Crutcher, R. M. 2008, ApJ, 680, 457

Truelove, J. K., Klein, R. I., McKee, C. F., Holliman, J. H., Howell, L. H., & Greenough, J. A. 1997, ApJ, 489, L179

Ward-Thompson, D., Motte, F., & André, P. 1999, MNRAS, 305, 143

Table 1.   Initial conditions and results for initially prolate cores. In this table and the following, ρ_0/ρ_R is the initial ratio of the central to the boundary density, the units for the initial angular velocity Ω_i are rad s^{-1}, and the magnetic braking factor f_{mb} is dimensionless. The final times t_f are given in units of the initial free fall time $t_{ff} = (3\pi/32G\rho_0)^{1/2} = 4.7 \times 10^4$ yr. Q denotes a core that collapses to form a quadruple system, B denotes a binary outcome, BB a binary-bar, and SB a single-bar. The results obtained by Boss (2002) for identical cores but without magnetic braking are shown as well.

model	ρ_0/ρ_R	Ω_i	f_{mb}	t_f/t_{ff}	result	Boss(2002)
P2BA	20:1	1.0×10^{-13}	0.001	4.649	Q	B
P2BB	20:1	1.0×10^{-13}	0.0001	4.683	Q	B
P2BC	20:1	3.2×10^{-14}	0.001	4.602	B	B
P2BD	20:1	3.2×10^{-14}	0.0001	4.603	B	B
P2BE	20:1	1.0×10^{-14}	0.001	4.833	BB	B
P1BA	100:1	1.0×10^{-13}	0.001	9.065	SB	B
P1BB	100:1	1.0×10^{-13}	0.0001	9.071	SB	B
P1BC	100:1	3.2×10^{-14}	0.001	8.942	SB	B
P1BD	100:1	3.2×10^{-14}	0.0001	8.945	SB	B
P1BE	100:1	1.0×10^{-14}	0.001	8.918	SB	B

Table 2.   Initial conditions and results for initially oblate cores. R denotes a ring formed, while NC means no significant collapse occurred.

model	ρ_0/ρ_R	Ω_i	f_{mb}	t_f/t_{ff}	result	Boss(2002)
O2BA	20:1	1.0×10^{-13}	0.001	4.565	NC	R
O2BB	20:1	1.0×10^{-13}	0.0001	2.456	R	R
O2BC	20:1	3.2×10^{-14}	0.001	2.127	R	Q
O2BD	20:1	3.2×10^{-14}	0.0001	2.134	R	Q
O2BE	20:1	1.0×10^{-14}	0.001	2.109	R	Q
O1BA	100:1	1.0×10^{-13}	0.001	4.656	R	R
O1BB	100:1	1.0×10^{-13}	0.0001	4.636	R	R
O1BC	100:1	3.2×10^{-14}	0.001	4.521	R	R
O1BD	100:1	3.2×10^{-14}	0.0001	4.495	R	R
O1BE	100:1	1.0×10^{-14}	0.001	4.422	R	Q

RHOMAX= −17.7   CONDIF=   0.1   R= 0.10E+18
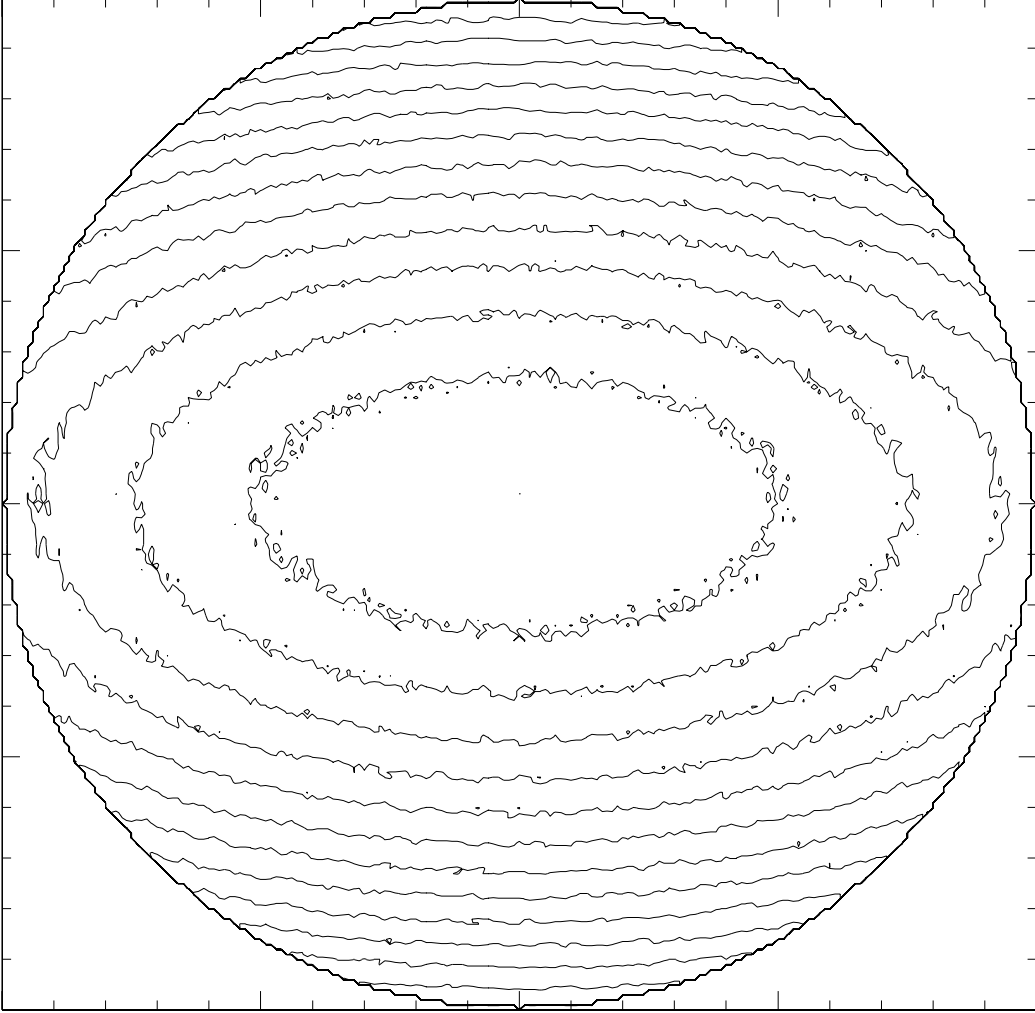
Fig. 1.— Initial equatorial density contours for prolate core models with 20:1 density contrasts. Maximum density is 2.0×10^{-18} g cm^{-3}. Contours represent changes by a factor of 1.3 in density. Region shown is 1.0×10^{17} cm in radius.
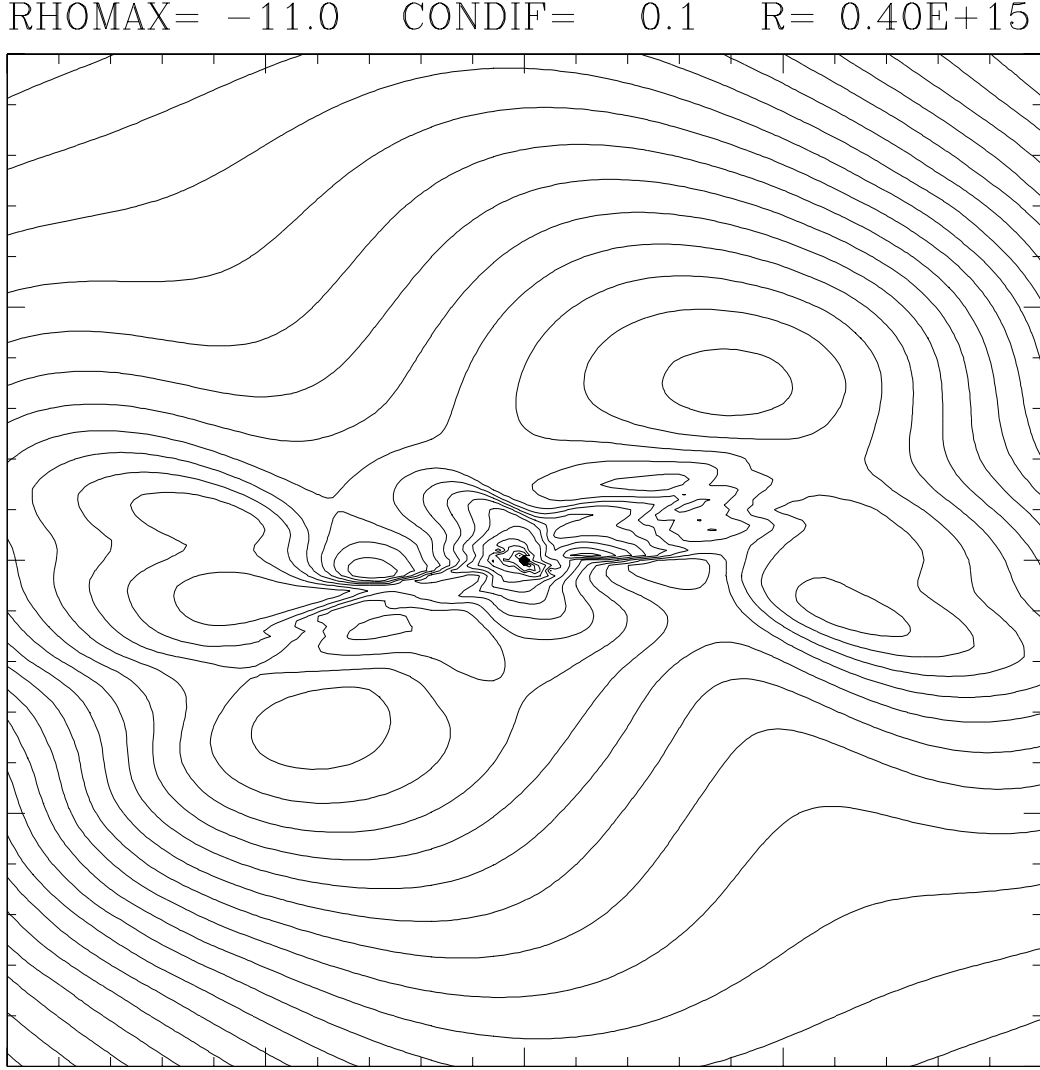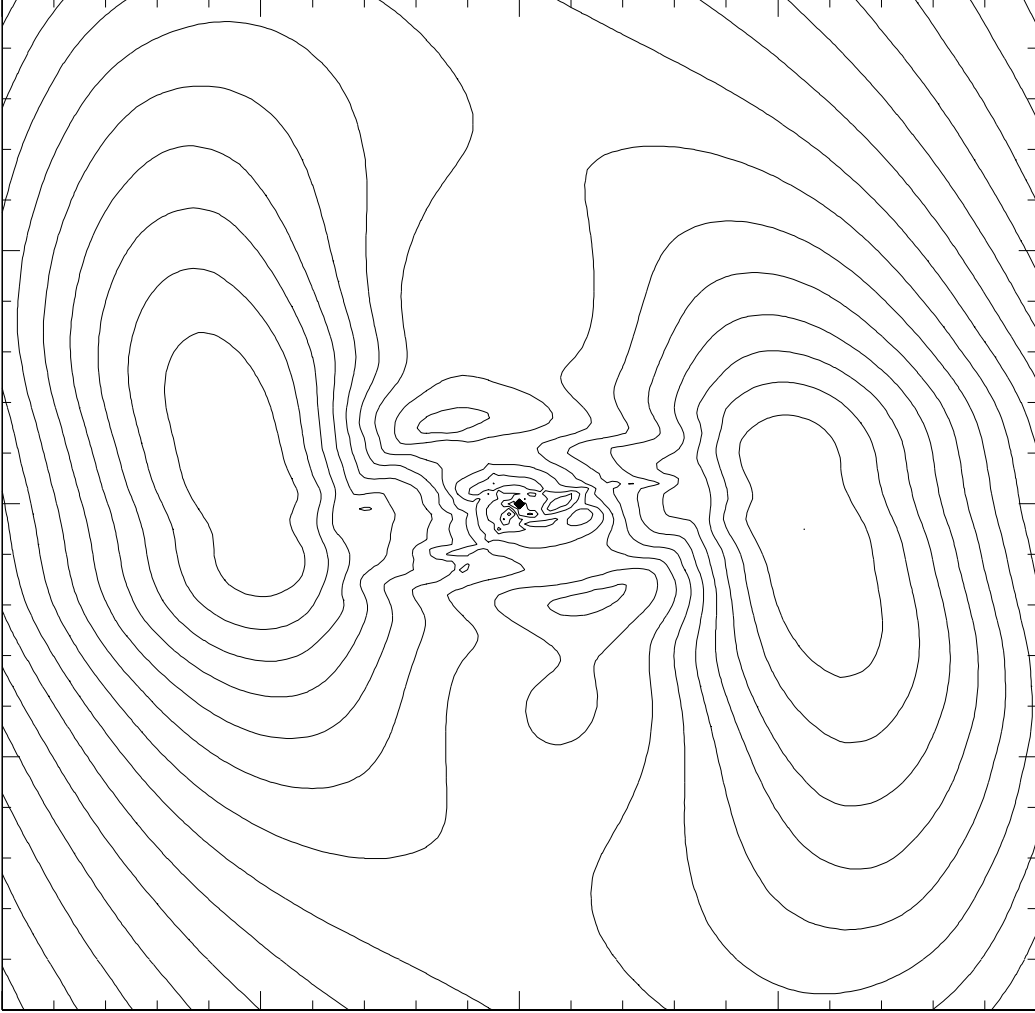
RHOMAX= −11.0   CONDIF=   0.1   R= 0.40E+15

Fig. 2.— Equatorial density contours for model P2BB at a time of 4.683 t_{ff}. Maximum density is 1.0×10^{-11} g cm^{-3}. Contours represent changes by a factor of 1.3 in density. Region shown is 4.0×10^{14} cm in radius. A possible quintuple protostellar system has formed: a central density maximum surrounded by four density maxima.

RHOMAX= −11.9   CONDIF=   0.1   R= 0.40E+15

Fig. 3.— Equatorial density contours for model P2BD at a time of 4.603 t_{ff}. Maximum density is 1.3×10^{-12} g cm^{-3}. Contours represent changes by a factor of 1.3 in density. Region shown is 4.0×10^{14} cm in radius. A binary protostellar system has formed.

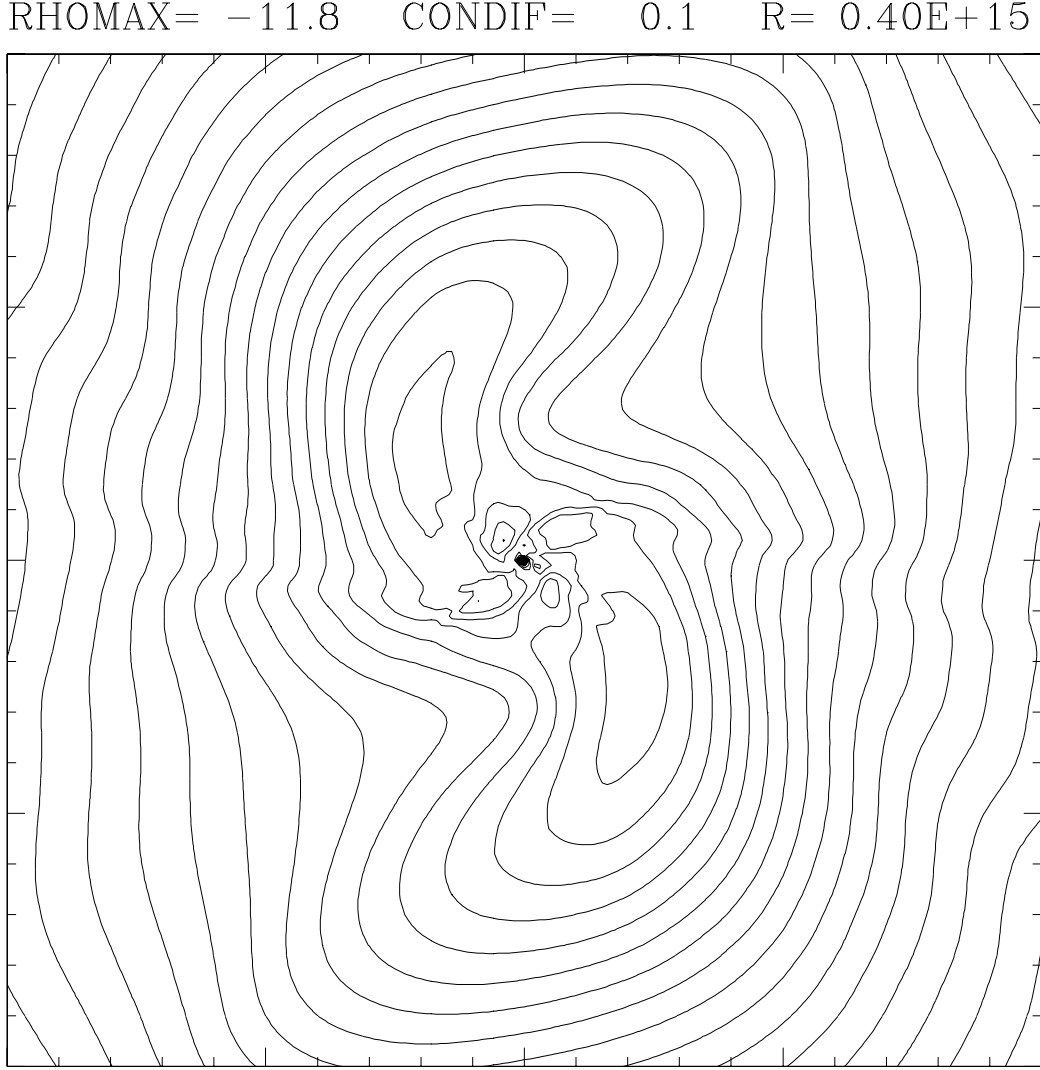RHOMAX= −11.8   CONDIF=   0.1   R= 0.40E+15

Fig. 4.— Equatorial density contours for model P2BE at a time of 4.833 t_{ff}. Maximum density is 1.6×10^{-12} g cm^{-3}. Contours represent changes by a factor of 1.3 in density. Region shown is 4.0×10^{14} cm in radius. A binary-bar system with four different local density maxima has formed.
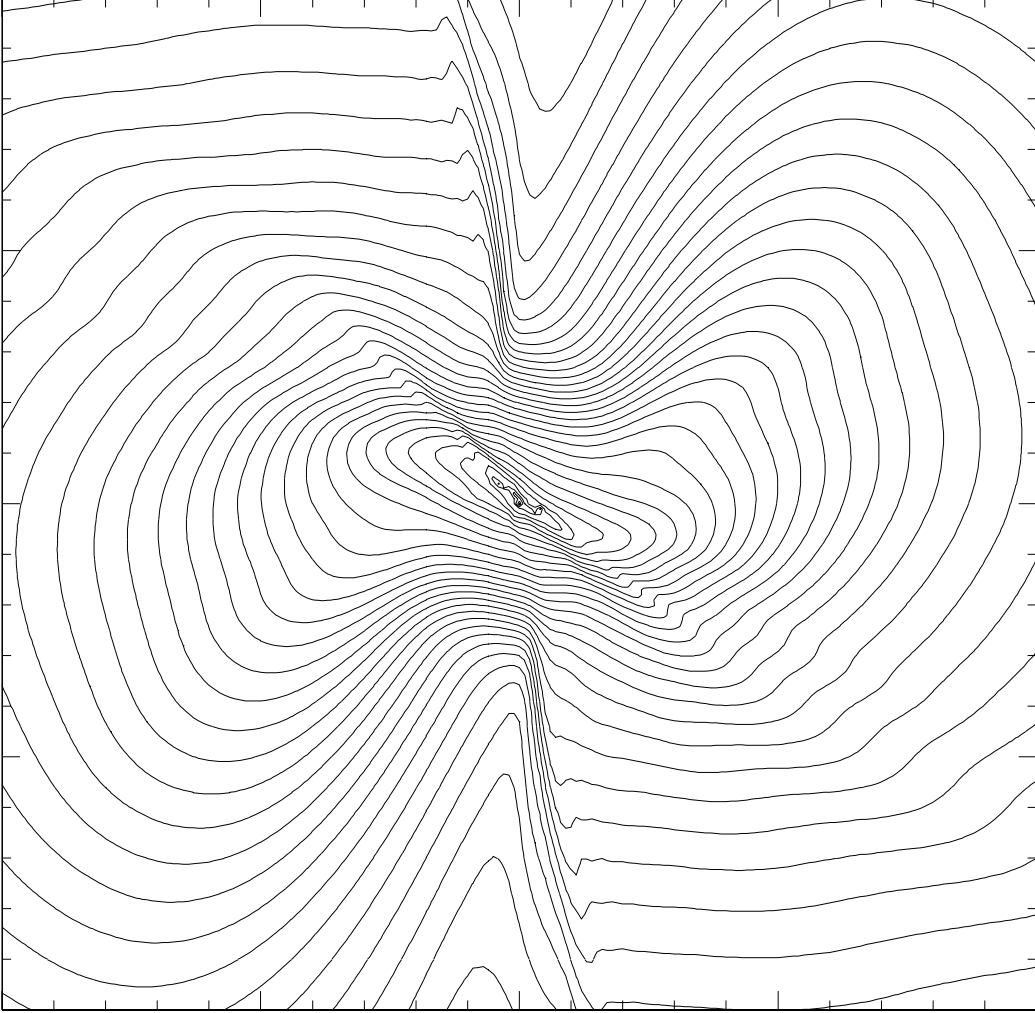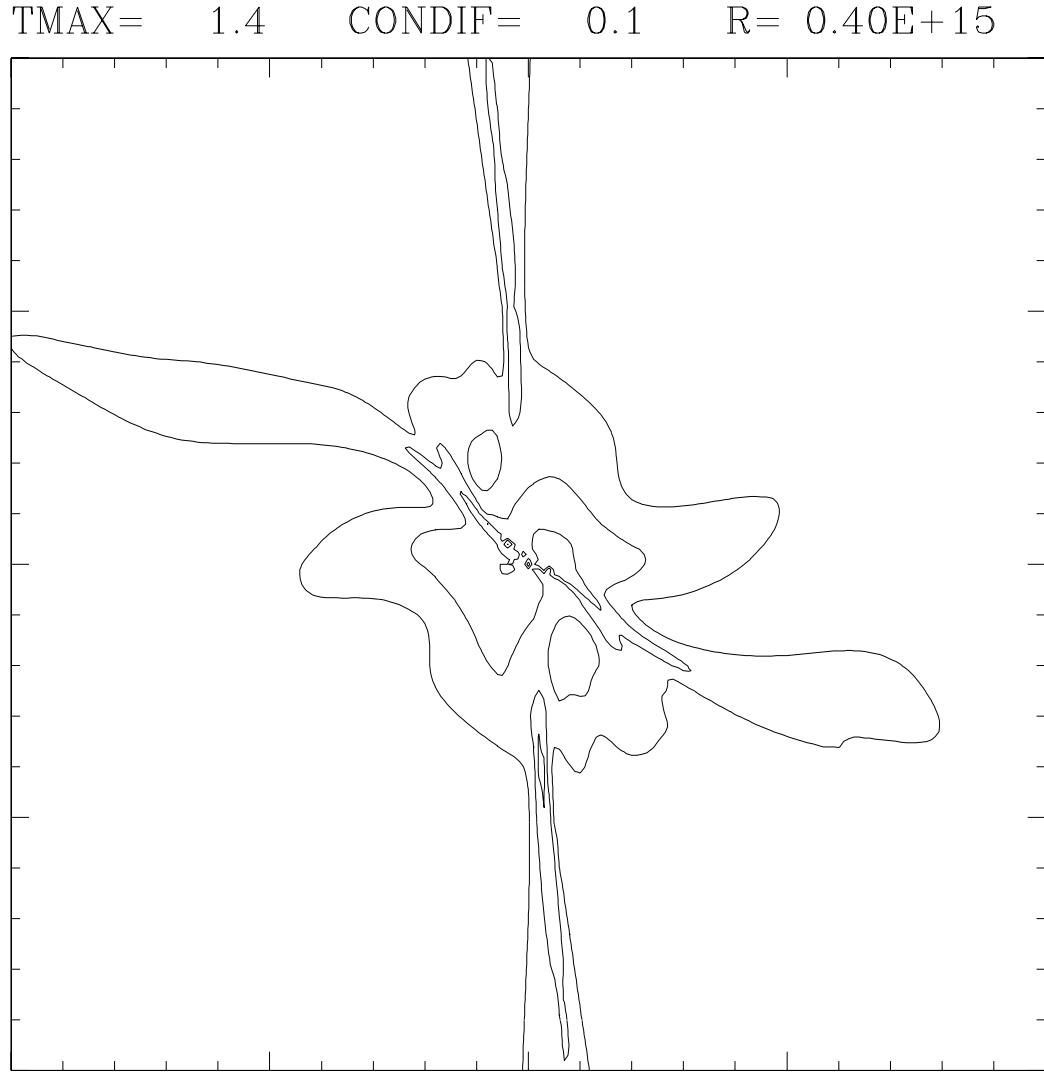
RHOMAX= −11.2   CONDIF=   0.1   R= 0.40E+15

Fig. 5.— Equatorial density contours for model P1BB at a time of 9.069 t_{ff}. Maximum density is 6.3×10^{-12} g cm^{-3}. Contours represent changes by a factor of 1.3 in density. Region shown is 4.0×10^{14} cm in radius. A single-bar system has formed.

TMAX=   1.4   CONDIF=   0.1   R= 0.40E+15

Fig. 6.— Equatorial temperature contours for model P1BB at a time of 9.069 t_{ff}. Maximum temperature is 25 K. Contours represent changes by a factor of 1.3 in temperature. Region shown is 4.0×10^{14} cm in radius.
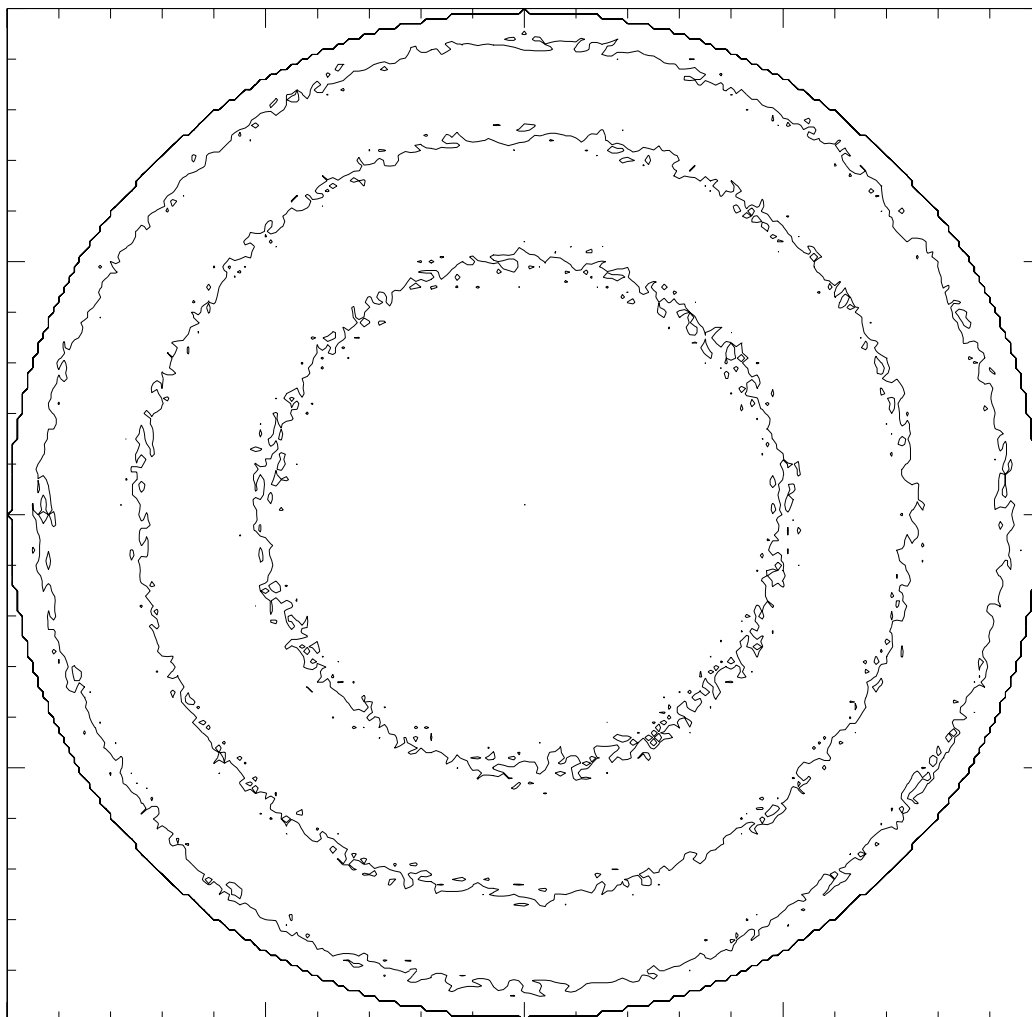
Fig. 7.— Initial equatorial density contours for oblate core models with 20:1 density contrasts. Maximum density is 2.0×10^{-18} g cm^{-3}. Contours represent changes by a factor of 1.3 in density. Region shown is 1.0×10^{17} cm in radius.
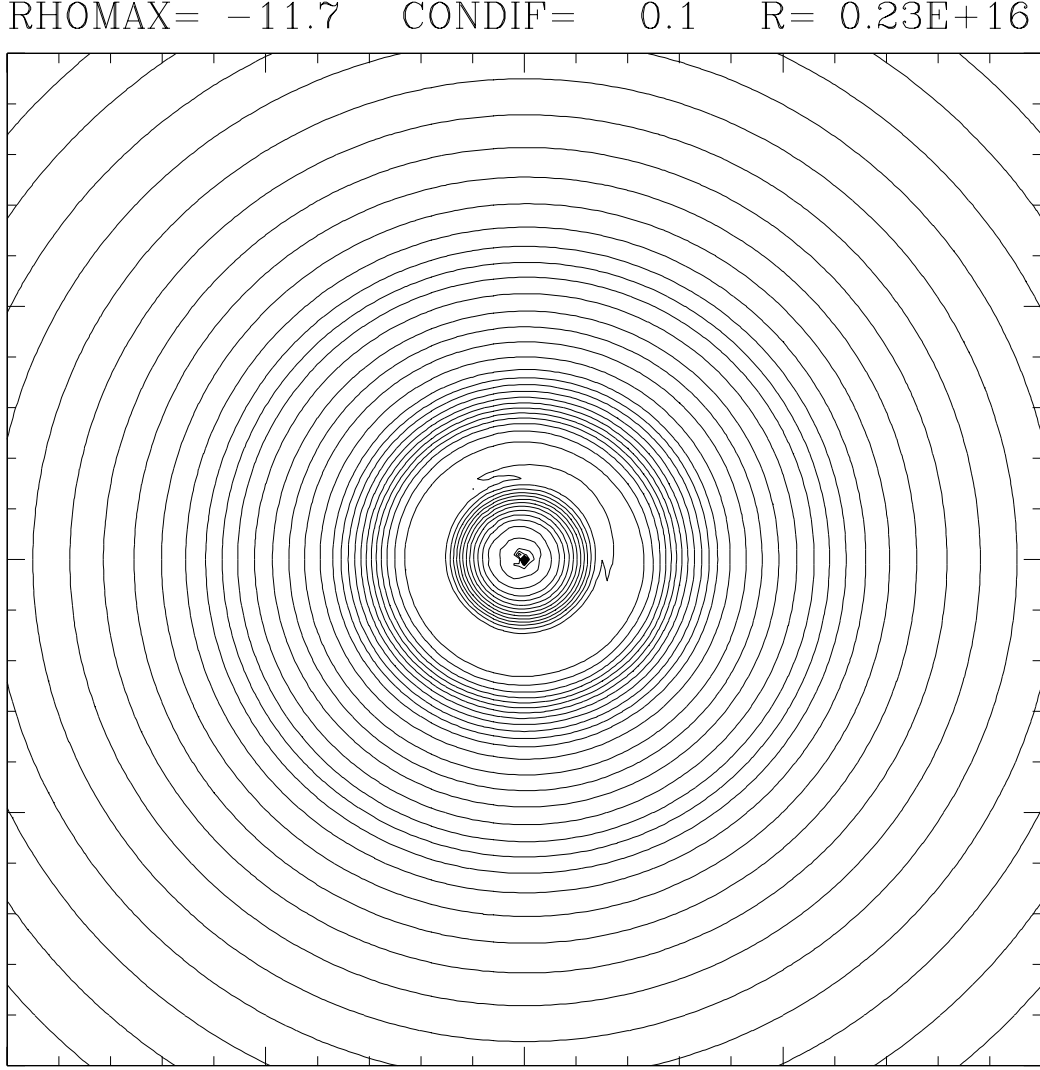
RHOMAX= −11.7   CONDIF=   0.1   R= 0.23E+16

Fig. 8.— Equatorial density contours for model O2BB at a time of 2.456 t_{ff}. Maximum density is 2.0×10^{-12} g cm^{-3}. Contours represent changes by a factor of 1.3 in density. Region shown is 2.3×10^{15} cm in radius. A ring has formed: a strong density minimum occurs at the center of the core.